



RESEARCH LETTER

10.1002/2015GL064229

Key Points:

- A downward parallel electric field develops to maintain charge quasi-neutrality
- In the upward FAC region, the parallel electric field can sometimes be upward
- The polar rain electron energy sometimes ramps up before reaching a plateau

Correspondence to:

S. Wing,
simon.wing@jhuapl.edu

Citation:

Wing, S., D. H. Fairfield, J. R. Johnson, and S.-I. Ohtani (2015), On the field-aligned electric field in the polar cap, *Geophys. Res. Lett.*, 42, 5090–5099, doi:10.1002/2015GL064229.

Received 14 APR 2015

Accepted 27 MAY 2015

Accepted article online 29 MAY 2015

Published online 7 JUL 2015

On the field-aligned electric field in the polar cap

Simon Wing¹, Donald H. Fairfield², Jay R. Johnson³, and Shin-I. Ohtani¹

¹The Johns Hopkins University Applied Physics Laboratory, Laurel, Maryland, USA, ²Space Weather Laboratory, NASA Goddard Space Flight Center, Greenbelt, Maryland, USA, ³Plasma Physics Laboratory, Princeton University, Princeton, New Jersey, USA

Abstract The Johns Hopkins University Applied Physics Laboratory open-field line particle precipitation model predicts downward field-aligned electric field to maintain charge quasi-neutrality. Previous studies confirmed the existence of such electric fields. However, the present study shows that upward field-aligned electric field can be found within upward field-aligned current (FAC) region. In the upward FAC region, upward electric field that accelerates electron downward is seen with the occurrence rates of 82%–96%. In contrast, the occurrence rates in the downward FAC regions are 3%–11%. Polar rain electrons located in the upward FAC region adjacent to closed field lines often show a ramping up of energy with increasing latitude before reaching a plateau. This plateau may be attributed to the magnetosheath electrons that progressively have higher antisunward velocity and lower density with increasing distance from the subsolar point before they asymptotically reach the solar wind values.

1. Introduction

It is well known that the Earth's magnetic field can reconnect with the interplanetary magnetic field (IMF) on the dayside. As a result, the magnetosheath or shocked solar wind plasma can enter the magnetosphere and a fraction of the magnetosheath particles precipitate into the ionosphere.

Because magnetosheath electrons can enter the magnetosphere more readily than ions, downward field-aligned electric fields must develop to restrict electron entries in order to maintain charge quasi-neutrality. At the Johns Hopkins University Applied Physics Laboratory, Wing *et al.* [1996, 2001, 2005] developed an open-field line particle precipitation model (APL-OPM) to model precipitating ions and electrons in the open-field line low-latitude boundary layer (open LLBL), cusp, mantle, and the low-latitude portion of the polar rain. For the southward IMF condition, the model retarding field-aligned potential drop resulting from maintaining charge quasi-neutrality in these four regions is plotted in Figure 1a. Immediately after the dayside reconnection, in the open LLBL, the solar wind ions and electrons can rush into the newly opened field line, but the electrons, having higher speeds, can move ahead of the ions and enter the magnetosphere in a greater proportion than the ions. As a result, retarding potential drop arises to limit some of the electron entries. A short time later, in the cusp, the bulk of the ions and electrons can enter the magnetosphere. So only a small or no potential drop is needed to maintain charge quasi-neutrality because the electrons and ions already maintain charge quasi-neutrality in the magnetosheath. As the field lines continue to $\mathbf{E} \times \mathbf{B}$ convect to the nightside, in the mantle, fewer ions can enter the magnetosphere because of increasing tailward speed. Hence, the potential drop slowly rises with increasing latitude to prevent electrons from entering the magnetosphere. Finally, in the polar rain, the entry points are further tailward where few ions can enter, and the potential drop increases to a higher level to prevent more electrons from entering the magnetosphere. In fact, the potential drop is so high that only solar wind suprathermal (strahl) electrons, having higher temperatures, can overcome the retarding potential drop to enter the magnetosphere largely unimpeded [Fairfield and Scudder, 1985]. The APL-OPM model uses a T96 magnetic field model [Tsyganenko and Stern, 1996], which is valid only to $X = -50$ Earth radii (R_E) and hence the model cannot model polar rain electrons of the central polar cap that enter $X < -50 R_E$.

Observational studies found retarding potential drops that are consistent qualitatively with the prediction of the APL-OPM [e.g., Wing *et al.*, 1996; Fairfield *et al.*, 2008]. However, Fairfield *et al.* [2008] found evidence that solar wind electrons occasionally go through a net accelerating potential drop before reaching the ionosphere. The present study investigates further field-aligned electric fields in the polar cap that affect the precipitating solar electrons.

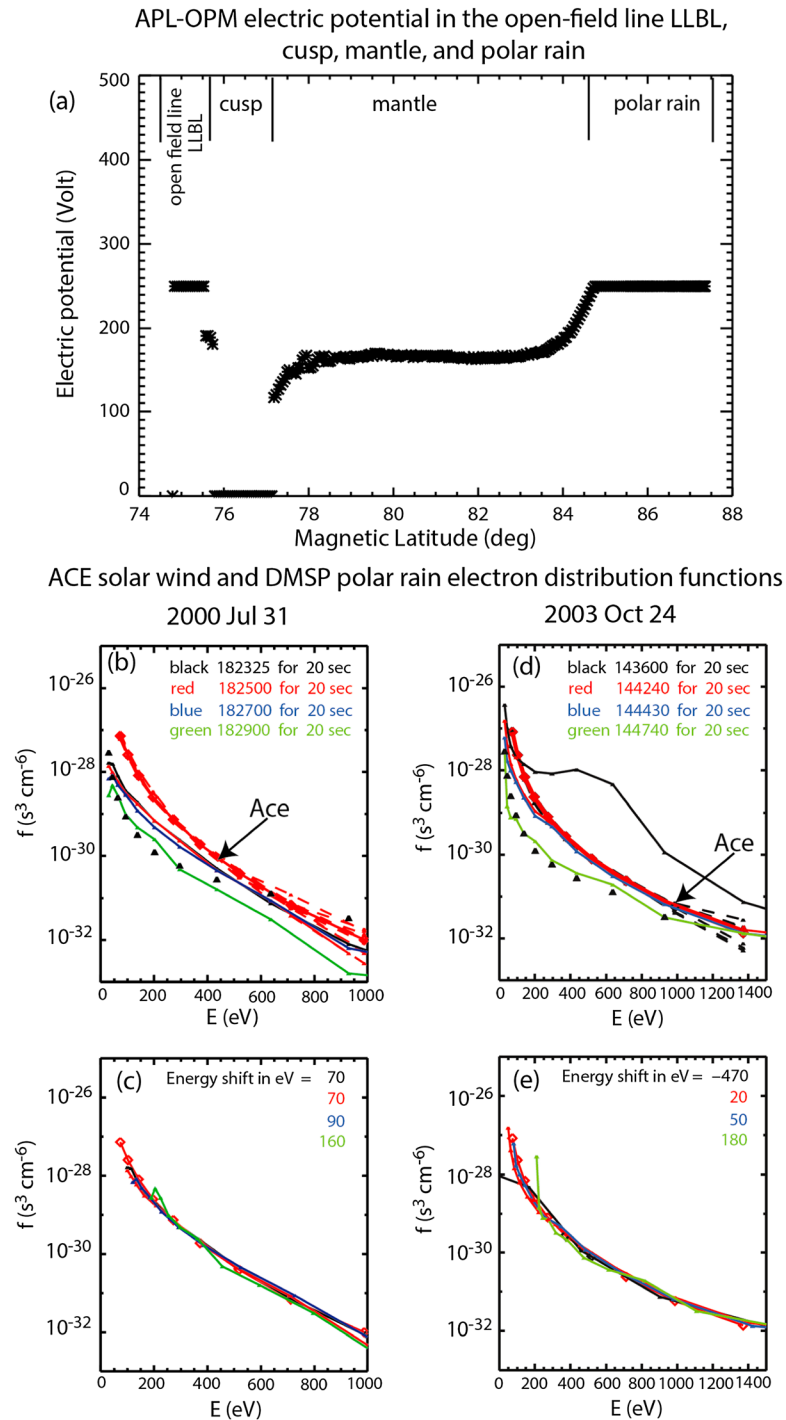


Figure 1. (a) Retarding field-aligned potential that arises to keep magnetosheath electrons from entering the magnetosphere in order to maintain charge quasi-neutrality. This potential is obtained from APL-OPM for southward IMF condition [Wing *et al.*, 1996, 2005]. (b) ACE solar wind and DMSP F13 polar rain electron distribution functions plotted versus energy for 31 July 2000 event. Field-aligned ACE data are shown by the heavy red trace while DMSP data from four different intervals are shown by the four thinner traces in black, red, blue, and green. Black triangles indicate the one count level for DMSP data. (c) Same as in Figure 1b except that the DMSP data are shifted to the right to best overlay ACE data. The shifts suggest that the electrons have gone through a net retarding field-aligned potentials (positive values), and their magnitudes are indicated. (d and e) The same as Figures 1b and 1c but for the 24 October 2003 event. In Figures 1d and 1e, the 14:36:00 UT distribution function (black line) is an anomaly because the field-aligned potential is an accelerating potential (negative value). All other distribution functions in the 31 July 2000 and 24 October 2003 events have positive field-aligned potentials, qualitatively consistent with Wing *et al.*'s [1996, 2005] results. Figure 1a is adapted from Wing *et al.* [2005], while Figures 1b and 1c are adapted from Fairfield *et al.* [2008].

Field-aligned electric field in the polar cap

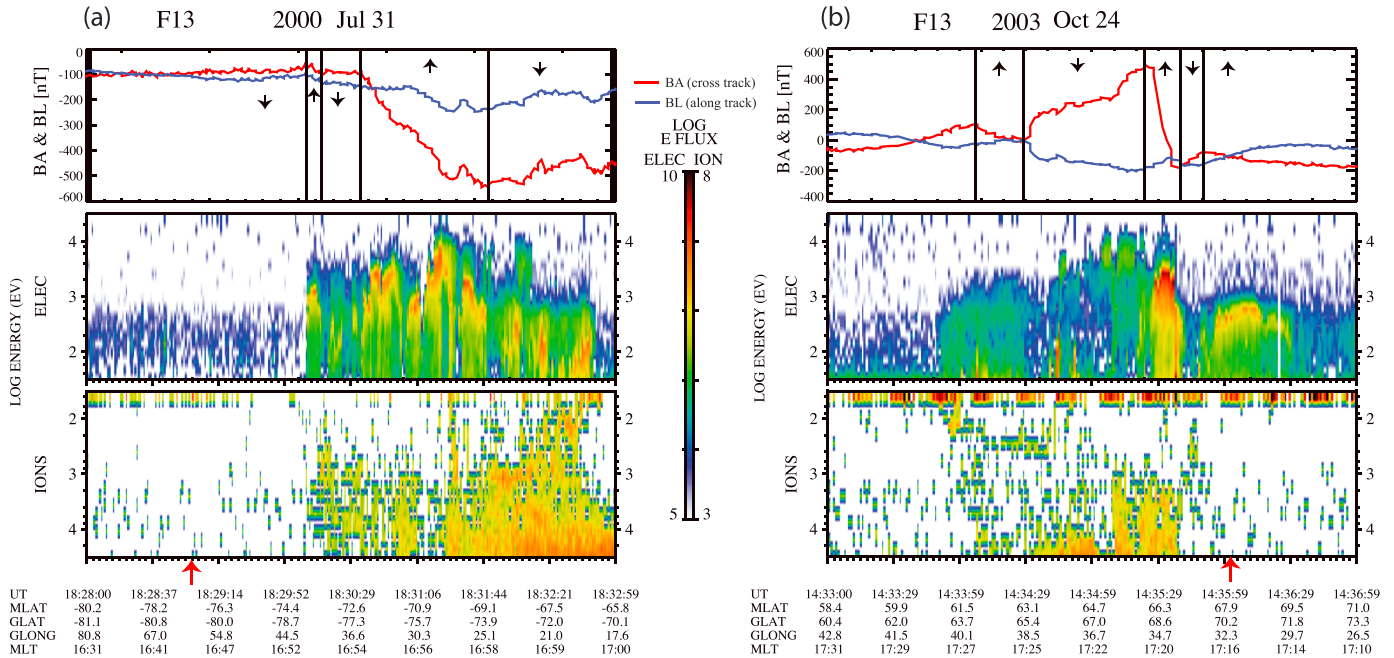


Figure 2. DMSF magnetic field and particle precipitation observations for the two events presented in Figure 1: (a) 31 July 2000 and (b) 24 October 2003. Figures 2a (top) and 2b (top) show the DMSF magnetic field cross track (BA, red) and along track (BL, blue) components. The upward and downward field-aligned currents are indicated by the up and down arrows, respectively. Figures 2a and 2b show the electron and ion spectrograms showing log differential energy flux, in units of $\text{eV}/\text{cm}^2 \text{sr eV}$, from 30 eV to 30 keV. The ion energy scale is inverted. In Figure 2a the polar rain is located in the weakly downward FAC region, and there is no evidence of monoenergetic electrons. In fact, at 18:29:00 UT (indicated by the red arrow at the bottom of Figure 2a), the retarding potential is 160 V (the green curve in Figures 1b and 1c). In contrast, in Figure 2b there is evidence of monoenergetic electrons in the polar rain where FAC is upward. At 14:36:00 UT (indicated by the red arrow in Figure 2b (bottom)), the electron differential energy flux peaks at about 500 eV, consistent with the accelerating potential of 470 V obtained in Figure 1e. The magnetic coordinates are obtained from Altitude Adjusted Corrected Geo-Magnetic Coordinates [Baker and Wing, 1989].

2. Downward and Upward Field-Aligned Electric Fields in the Polar Cap

In a study of variations in the otherwise uniform precipitation of solar wind electrons over the polar cap, Fairfield *et al.* [2008] plotted the solar wind electron phase space density obtained by ACE along with the corresponding polar rain electrons simultaneously measured at low altitude by DMSF satellites. They found that the DMSF polar rain spectra would usually match ACE solar wind electron spectra if the DMSF electrons were shifted up in energy. On occasion, however, the shift was in the opposite direction. Examples extracted from Fairfield *et al.* [2008] are shown in Figures 1b–1e for the 31 July 2000 and 24 October 2003 events. Figures 1b and 1d show the original measurements from ACE (heavy red trace) and DMSF (thinner colored lines). In Figures 1c and 1e, all traces, excepting the black trace in Figure 1d, have been shifted to the right (up in energy) implying that the solar wind electrons have gone through a net retarding potential drop before reaching DMSF altitudes. This result is consistent qualitatively with the predictions of APL-OPM. The black trace in Figure 1d that is shifted to the left (down in energy) in Figure 1e implies a net accelerating potential drop, which is the opposite of that predicted by Wing *et al.* [1996, 2001, 2005]. An upward field-aligned electric field sometimes arises in the upward field-aligned current (FAC) region when the electron density in the source region is too low to provide enough current carriers to carry the current [e.g., Knight, 1973].

To investigate this possibility, we examine the simultaneous observations of the DMSF magnetic field data [Rich *et al.*, 1985] and particle data (SSJ4/SSJ5) [Hardy *et al.*, 1984]. The upward pointing particle detectors measure the relevant electrons whose alignment within a few degrees of the magnetic field in the distant magnetosphere allows them to reach low altitude and experience field-aligned electric fields.

Figure 2a shows the 31 July 2000 event (the same event shown in Figures 1b and 1c) when IMF $(B_x, B_y, B_z) \sim (4, -4, -8)$ nT. Figure 2a (top) shows up and down arrows indicating the polarities of the field-aligned currents that are derived from the cross-track component (red line), assuming infinite current

sheet [e.g., Iijima and Potemra, 1976; Wing et al., 2010]. The poleward boundary of the auroral oval is located at about magnetic latitude (MLAT) $\sim -73.2^\circ$ (18:30:12 UT). The polar rain, which is located poleward of MLAT $\sim -73.2^\circ$, looks like the typical polar rain, showing no evidence of electron acceleration. This is consistent with the magnetic field observations that indicate that FAC is either small or downward.

In Figure 1c, the shifted green distribution function for 18:29:00 UT (for the electron spectra marked by the red arrow in Figure 2a) indicates that the net retarding potential drop is 160 V. This potential drop is qualitatively consistent with the potential drop needed to maintain charge quasi-neutrality in APL-OPM as shown in Figure 1a. In the model, the potential drop has dependencies on the solar wind density and temperature. Ion and electron outflows, which are absent in the model, may affect the charge quasi-neutrality calculation and can complicate model-data comparisons, as discussed next. In any case, the net potential drop in the polar rain has been observed to range from several tens to hundreds of volts [Fairfield et al., 2008].

The solar extreme ultraviolet (EUV) radiation can ionize the atmosphere, which leads to up flowing photoelectrons and the development of ambipolar upward electric fields at several hundreds of kilometers to a few R_E , which in turn drives ion outflows [e.g., Su et al., 1998]. Upward field-aligned electric fields can also develop in the upward field-aligned current region where the electrons need to overcome the mirror force around $1-3 R_E$ [Knight, 1973; Block and Fälthammar, 1991]. On the other hand, downward field-aligned electric fields should develop close to the magnetopause boundary to prevent the entry of excess solar wind electrons. Therefore, it is expected that the signatures of acceleration or deceleration may also reflect the differences in the location of the acceleration or deceleration.

Kitamura et al. [2012] studied upgoing and reflected photoelectrons and found that a small downward accelerating potential drop of 20 V exists most of the time at altitude above 3800 km. The existence of this accelerating potential drop at intermediate altitudes is not inconsistent with the simultaneous existence of a retarding potential drop at high altitude near the magnetopause. Thus, the retarding potential drop obtained by Fairfield et al. [2008] gives a lower bound estimate of the potential drop needed to maintain charge quasi-neutrality near the magnetopause.

Figure 2a can be contrasted to Figure 2b, which shows the DMSP observations for the 24 October 2003 event (the same event shown in Figures 1d and 1e) when IMF (B_x, B_y, B_z) $\sim (-6, -1, -7)$ nT. In Figure 2b, the poleward boundary of the auroral oval is located at MLAT $\sim 66.8^\circ$ (14:35:38 UT). In Figure 1e, the shifted black distribution function (14:36:00 UT) suggests that the net accelerating field-aligned potential drop is 470 V. The polar rain electron spectra corresponding to this distribution function are indicated by the red arrow in Figure 2b (bottom). The polar rain electrons at MLAT $\sim 67.7^\circ-69.5^\circ$ (14:35:55–14:36:30 UT) are monoenergetic electrons or electron acceleration events, which are consistent with the electrons having gone through an upward field-aligned electric field [e.g., Wing et al., 2013]. The magnetometer data indicate that these monoenergetic electrons are located in the upward FAC region. The accelerating potential drop obtained by Fairfield et al. [2008] (470 V) gives a lower bound estimate of the potential drop that exists at the acceleration region, $1-3 R_E$, because the electrons may have gone through retarding potential drops at the magnetopause.

Moreover, Figure 2b shows that at 14:36:00 UT the electron differential energy fluxes peak at about 500 eV, which would not be inconsistent with the accelerating potential drop of 470 V obtained in Figure 1e. The electrons with energies lower than ~ 500 eV, which have low fluxes, may be attributed to the ionospheric electron outflows that are turned around by the upward electric field. These ionospheric electrons correspond to the electrons having energies below 470 eV on the black curve in Figure 1d. In Figure 1e, part of the curve representing these electrons (which do not originate from solar wind) does not overlay the solar wind electron curve (the thick red curve), but the rest of the curve does.

Wing et al. [2010, 2011] report that it is not unusual to find upward field-aligned electric fields in the afternoon upward FAC region located within the boundary layer and open-field lines. Lyons [1980] notes that near the boundary layer on the duskside, the plasma flow is sunward and antisunward in the magnetosphere and magnetosheath, respectively, and the magnetospheric magnetic field has a northward component. As a result, the convective electric field converges ($\nabla \cdot E < 0$), which can lead to large-scale upward field-aligned current. Larger V_{sw} would generate larger upward FAC density ($J_{||}$), and if the electron density were not large enough, then an accelerating potential drop would develop to draw more electrons downward [e.g., Wing et al., 2011].

Polar rain electrons in the upward field-aligned current region

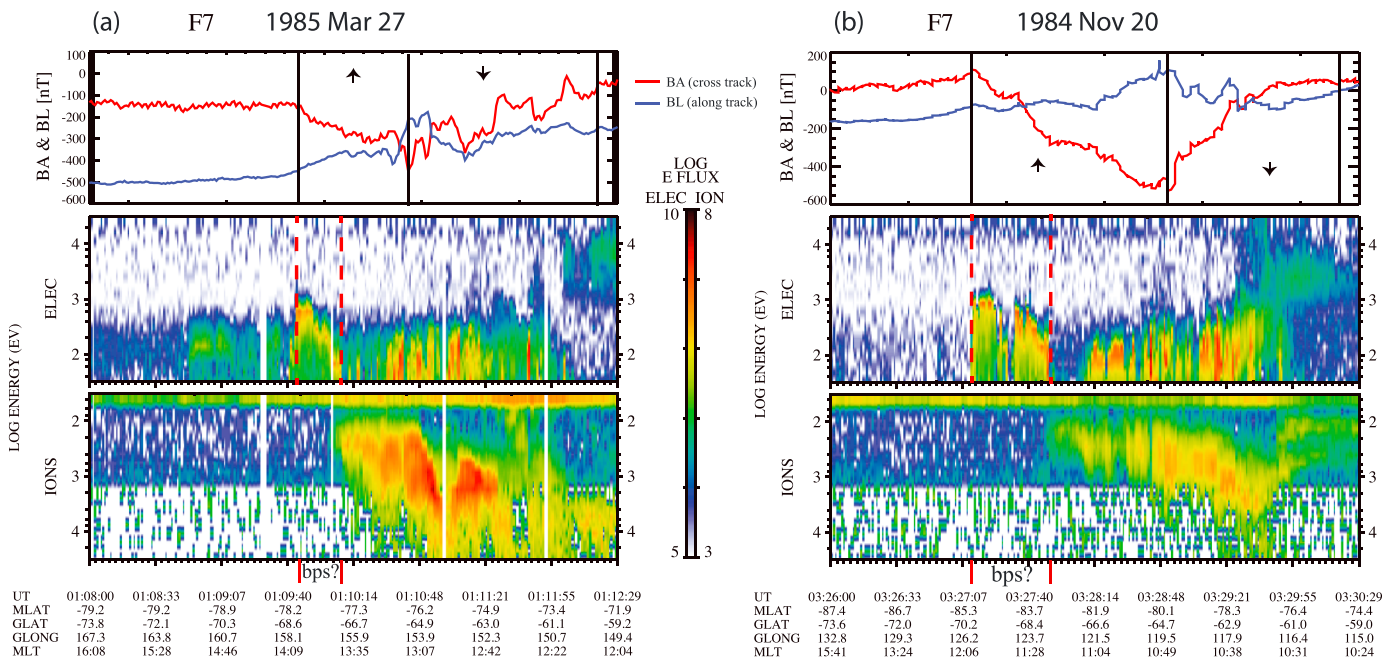


Figure 3. Two examples showing polar rain electron energy ramps up with increasing latitude before reaching a plateau. The format is the same as in Figure 2. In Figures 3a (top) and 3b (top) the arrows indicate the polarities of only large-scale field-aligned currents. At the poleward edge of the upward FAC region, between the two red vertical dashed lines, the polar rain electron energy ramps up with increasing latitude before reaching a plateau. Due to the high electron energies, the DMSP automatic algorithm often classifies this region as BPS, which is most likely incorrect (see text). The white vertical bands in Figure 3a indicate data gaps.

3. A Morphology of the Low-Latitude Polar Rain Electrons in the Upward FAC Region

In the upward FAC region, the low-latitude polar rain sometimes shows a ramping up of the electron energy with increasing latitude before reaching a plateau. Such structures are typically found slightly poleward of the dayside open-closed boundary. Two examples are presented (more examples can be found in *Wing et al.* [2010]). Unfortunately, solar wind data are not available for these two events.

Figure 3a shows the 27 March 1985 event in which DMSP F7 observes a double cusp [e.g., *Wing et al.*, 2001] at MLAT $\sim -74.7^\circ$ – -76.4° , a mantle at MLAT $\sim -76.4^\circ$ – -77.5° , and polar rain (prior to 01:10:09 UT). Immediately poleward of the mantle, the polar rain electron energies are typical, but at MLAT $\sim -77.7^\circ$ – -78.1° (between the two red vertical dashed lines in Figure 3a (middle)), the electron differential energy flux peak energy increases with increasing latitude before plateauing at just below 1 keV, which is higher than that of the typical of polar rain electrons. The magnetometer data indicate that the polar rain in this interval is located near the poleward edge of the upward FAC region. Poleward of MLAT $\sim 78.1^\circ$, the FAC suddenly weakens, and the polar rain electron energies and fluxes suddenly drop.

Figure 3b shows the DMSP F7 20 November 1984 pass that shows the same feature in the polar rain. The DMSP observes cusp at MLAT $\sim -77.4^\circ$ – -80.3° , mantle at MLAT $\sim -80.3^\circ$ – -83.2° , and polar rain (prior to 03:27:44 UT). At MLAT $\sim -83.2^\circ$ – -85.1° (between the two red vertical dashed lines in Figure 3b (middle)), the polar rain electron differential energy flux peak energy increases with increasing latitude before reaching a plateau at around 1 keV. The magnetometer data indicate that the polar rain in this interval is located near the poleward edge of the upward FAC region. The FAC changes from upward to slightly downward at MLAT $\sim -85.1^\circ$, which is accompanied by a sudden drop in the polar rain electron energies and fluxes. Poleward of MLAT $\sim -85.1^\circ$, the polar rain electrons look like the typical polar rain electrons, and FAC is small or slightly downward.

Following the reconnection at the magnetopause, the field lines would eventually convect to the nightside, while the magnetosheath plasma continuously enters the magnetosphere. The electrons from the higher-latitude polar rain originate from the magnetopause region that is further down the tail. Because of the evolution of the magnetosheath density and speed [e.g., *Spreiter and Stahara*, 1985], at progressively

higher latitude, polar rain electrons originate from the magnetosheath region that progressively has lower density and higher speed. *Wing et al.* [2011] and *Echim et al.* [2008] show that higher speed suggests higher velocity shear at the magnetopause boundary, which can increase field-aligned potential drop. The same studies also show that lower density can also increase field-aligned potential drop. These relations can also be seen in equation (1), as discussed below. As the magnetosheath speed increases and density decreases, the accelerating potential drop and polar rain electron differential energy flux peak energy progressively increase. Eventually, the magnetosheath density and velocity asymptotically reach their solar wind values, which may explain the plateauing of the polar rain electron differential energy flux peak energy.

Johnson and Wing [2015] presents a model for current-voltage relation at the magnetopause boundary layer and open-field lines. In the upward FAC regions the maximum accelerating potential drop can be estimated analytically [*Johnson and Wing*, 2015] as

$$\Delta\phi_{\parallel, \max} = \frac{J_{\parallel}}{\kappa} \approx \frac{V_0 B_0 \sqrt{b} L}{2 \left(1 + \frac{\Delta_m}{L \sqrt{b}} \right)} \quad (1)$$

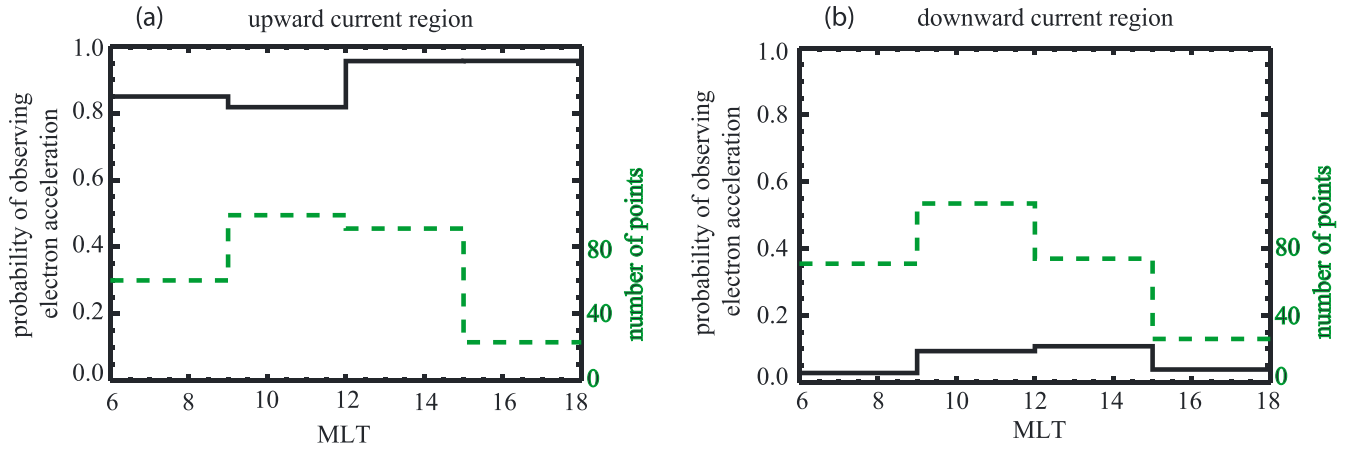
where $\Delta\phi_{\parallel}$ = field-aligned potential drop, L = electrostatic auroral scale length = $(\Sigma_p/\kappa)^{0.5}$, Σ_p = Pedersen conductivity, $\kappa = n_e e^2 / (2\pi m_e k_b T_e)^{0.5}$, V_0 = velocity shear at the boundary layer, B_0 = magnetic field magnitude at the boundary layer, $b = B_i/B_0$, B_i = ionospheric magnetic field magnitude, Δ_m = thickness of the boundary layer, n_e = electron number density, e = electron charge, m_e = electron mass, T_e = electron temperature, and k_b = Boltzman constant. This expression shows that as the magnetosheath flow speed or V_0 increases and n_e decreases, $\Delta\phi_{\parallel}$ increases. Assuming solar wind suprathermal $n_e = 0.4 \text{ cm}^{-3}$, $T_e = 1 \times 10^6 \text{ K}$, $V_0 = 400 \text{ km s}^{-1}$, $B_0 = 3 \text{ nT}$, $B_i = 4 \times 10^{-5} \text{ T}$, $\Delta_m = 6000 \text{ km}$, $\Sigma_p = 2 \text{ S}$, equation (1) predicts field-aligned potential drop of 1.3 keV. Figure 3 shows that in the 27 March 1985 and 20 November 1984 events, the electron differential energy flux peak energies plateau to about 1 keV, which is close to the theoretical prediction.

In Figure 3b, the upward FAC region at MLAT $\sim -79.9^\circ$ – -85.1° colocalizes with mantle and some polar rain regions. In the mantle region, at MLAT $\sim -81.8^\circ$ – -83.2° , the FAC weakens as evidenced by the reduction of the slope of the red line. This observation underscores a couple of points. First, the smaller FAC corresponds to smaller precipitating electron fluxes. Second, the electron energies in this interval look more similar to those in the polar rain poleward of MLAT $\sim -85.1^\circ$ (prior to 03:27:12 UT) than the electron energies that immediately follow, in the interval MLAT $\sim -83.2^\circ$ – -85.1° (between the two red vertical dashed lines). This supports our argument that the enhanced electron fluxes and energies in this interval are just the regular polar rain or mantle electrons that have gone through accelerating potential drop associated with upward FAC.

Newell et al. [1991a, 1991b, 1991c] developed automatic algorithm that classifies the dayside particle precipitation source regions. This algorithm does not take into account the effect of FACs. Often, this algorithm would classify the regions between the two red vertical dashed lines in Figure 3 as boundary plasma sheet (BPS), which is a closed field line region. In Figure 3b, the algorithm labels the sequence of boundaries from low to high latitude as central plasma sheet-BPS-cusp-mantle-BPS-polar rain. If this were correct, then this would suggest a rather unusual scenario where, from low to high latitude, the field lines are closed-open-closed-open. A more likely scenario is that the BPS that is located poleward of the mantle is misclassified because the mantle or polar rain electrons have gone through upward field-aligned electric field in the upward FAC region and gained enough energy to make their spectra look more similar to those of BPS rather than mantle or polar rain. Thus, taking the upward electric field into account, we would have the expected pattern from low to high latitude as closed-open field lines. (This correction should also apply to the examples presented in Figures 1a, 1b, and 7 in *Wing et al.* [2010].) Moreover, in the electron acceleration region, there is no significant ion precipitation. In fact, the ions look similar to those in the adjacent polar rain region. Taken together, the present study and *Wing et al.* [2010] suggest that the *Newell et al.* [1991a, 1991b, 1991c] algorithm needs to be modified by taking into account FAC observations.

Without the help of imagers, it is hard to determine whether the electron accelerations in the polar cap in Figure 3 are related to polar cap arcs [*Zhu et al.*, 1997]. Some polar cap arcs are thought to originate from plasma sheet because they are accompanied by the plasma sheet ion precipitation [*Hoffman et al.*, 1985; *Milan et al.*, 2005]. In this case, a DMSF traveling poleward across the polar region would indeed observe particle precipitation structure that suggests closed-open-closed-open field lines. However, in Figure 3,

The probability of observing electron acceleration in the polar cap



Examples of electron acceleration in the downward FAC region

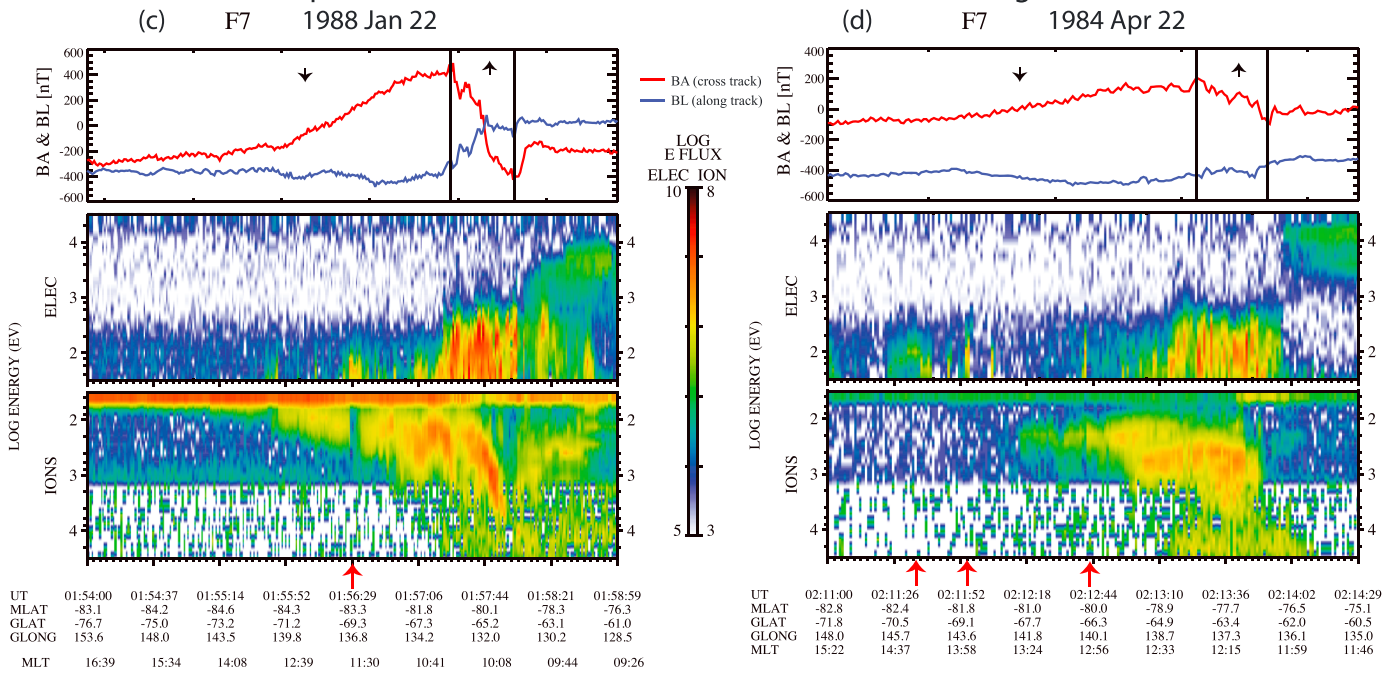


Figure 4. The probability of observing electron acceleration in the polar cap plotted as a black solid line in (a) upward current region and in (b) the downward current region. The number of points in each 3 h bin is plotted as a green dashed line. (c and d) Two examples of electron acceleration events in the downward FAC regions are presented for 22 January 1988 and 22 April 1984 events, respectively, in the same format as in Figure 2. The electron acceleration intervals are indicated by the red arrows at the bottom panel.

the electron accelerations in the polar cap are not accompanied by significant precipitating ions—the ions certainly do not look like the typical plasma sheet ions [e.g., *Wing and Newell, 1998*]. If the electron accelerations in Figure 3 were polar cap arcs, they may be similar to the ones reported in *Burke et al. [1982]*, which shows discrete arcs associated with electrons having gone through ~1 kV potential drop within upward FAC regions that are located on open-field lines.

4. The Occurrence of the Upward Field-Aligned Electric Fields in the Polar Cap

The occurrence of the upward field-aligned electric fields in the polar cap in the upward and downward dayside FAC regions from 06 to 18 magnetic local time (MLT) is investigated. About 300 upward and downward FAC events are randomly chosen from DMSP F7 1984–1987 and DMSP F12 1995–2001 observations. The dayside polar cap regions include cusp, mantle, polar rain, and LLLBL. After discarding events with bad data points or

events with no simultaneous magnetic field and particle observations, there are 273 and 278 for upward and downward FAC events, respectively. The presence of the electron acceleration is used as evidence for the presence of upward field-aligned electric field. Here the electron accelerations are not necessarily polar cap arcs, and the term electron acceleration indicates monoenergetic electrons that occur either alone or in combination with broadband electrons [Wing *et al.*, 2013]. An example of the latter in the closed field line (although closed field line is not the focus of the present study) is shown in Figure 2b at MLAT $\sim 66.1^{\circ}$ – 66.9° (14:35:25–14:35:40 UT) where the electrons may have been heated and accelerated by waves rather than strictly by the upward field-aligned electric field alone [Wing *et al.*, 2013].

Figures 4a and 4b present the probability of observing any electron acceleration in the upward and downward FAC regions, respectively. Figure 4a shows that the probability of observing electron acceleration in the upward FAC region is quite high, 0.82 to 0.96, depending on the MLT. In contrast, the probability of observing electron acceleration in the downward FAC region is much lower, 0.03 to 0.11.

Many data points do not have associated simultaneous IMF observations. For those events that have simultaneous IMF observations, in the upward FAC regions (Figure 4a), 92 out of 176 electron acceleration events (52%) are associated with northward IMF. In the downward FAC regions (Figure 4b), 7 out of 10 electron acceleration events (70%) are associated with northward IMF. Taking into account the sample sizes, statistically, there is no clear strong preference for north-south orientation of IMF in both distributions. This needs to be investigated further.

Figures 4c and 4d show two examples of electron acceleration in the downward FAC regions (the solar wind observations are not available). The electron acceleration intervals are indicated by the red arrows at Figures 4c (bottom) and 4d (bottom). In Figure 4c, the precipitating ion fluxes accompanying the electron accelerations are lower than the surrounding regions, which perhaps can be attributed, at least partly, to the upward field-aligned electric field.

Sometimes, electron acceleration can also be found in weak or no FAC region. An example can be seen in Figure 3a, which shows monoenergetic electrons (differential energy fluxes peak ~ 150 eV) between 01:08:51 and 01:09:02 UT.

It is not clear what mechanism(s) can lead to electron acceleration in the downward or no FAC regions. Broadband acceleration in upward, downward, or no FAC regions can be attributed to small-scale dispersive Alfvén waves that create time-varying field-aligned electric field that disperses electron energy [e.g., Chaston *et al.*, 2002; Watt and Rankin, 2009; Wing *et al.*, 2013]. On the other hand, monoenergetic electrons are usually attributed to quasi-static potential drops, which are typically associated with upward FAC regions and global magnetic field configuration or low-frequency waves [Damiano and Johnson, 2012]. However, it is not clear what causes monoenergetic electron in downward or no FAC regions. The strahl electrons may be accelerated in the heliosphere. This topic will be further investigated in the future.

5. Summary and Conclusion

The present study investigates the field-aligned electric fields in the polar cap region adjacent to the auroral oval. APL-OPM predicts upward field-aligned electric field to retard electron entries into the magnetosphere in order to maintain charge quasi-neutrality. Such electric fields have been confirmed in a previous study that fitted DMSP spectra as well as in a study that compared ACE and DMSP electron distribution functions. However, field-aligned electric field with the opposite polarity can be occasionally found in the upward FAC region. Near the boundary layer on the duskside, there are discontinuities in convection electric field such that $\nabla \cdot E < 0$, which can generate large-scale upward FACs, which may require upward field-aligned electric field to draw more electrons downward when the electron density is too low. Generally, in the upward FAC region, upward electric fields that accelerate electrons downward are seen with the occurrence rates of 82%–96%, depending on the MLT, with no clear preference for IMF B_z . In contrast, the occurrence rates in the downward FAC regions are 3%–11%, but it is not clear what mechanism(s) create upward electric field in the downward or no FAC region. The APL-OPM does not take into account the effects of FAC and ionospheric outflows on field-aligned electric field.

The location of the upward and downward field-aligned electric fields may differ. Downward field-aligned electric fields should develop close to the magnetopause boundary to prevent the entry of excess

electrons, while upward field-aligned electric fields are typically largest at lower altitude where they are required to overcome the mirror force.

The polar rain electrons located in the upward FAC region often show a ramping up of energy with increasing latitude. This may be attributed to evolution of the magnetosheath electrons that progressively have higher antisunward velocity and lower density with increasing distance from the subsolar point. At progressively higher latitude, the polar rain electrons originate from magnetosheath region that has higher antisunward velocity and lower density, both of which can increase upward accelerating potential drop. This would continue until the magnetosheath velocity and density asymptotically reach those of solar wind, at which point the potential drop would plateau. As a result, the precipitating electron characteristic energy would also plateau. At latitudes poleward of the upward FAC region where the FAC is nearly zero or downward, polar rain electrons enter even further down the tail, but they do not undergo such acceleration [Fairfield and Scudder, 1985].

The DMSP automatic particle precipitation classification algorithm does not take into account the effect of upward field-aligned electric field. As a result, the algorithm can misclassify mantle or polar rain (with no significant ion precipitation) as BPS, leading to an unusual scenario where the magnetic field lines would be closed-open-closed-open from low to high latitude. Taking into account the electron acceleration in the upward FAC region, one would get the expected scenario of closed-open field lines from low to high latitude.

Acknowledgments

The Air Force Research Laboratory has been helpful in the acquisition of DMSP SSJ4/SSJ5 and magnetometer data, as has the World Data Center in Boulder, Colorado. NASA OMNIWeb Plus (<http://omniweb.gsfc.nasa.gov/>) provides the solar wind data. All the derived data products in this paper are available upon request by e-mail (simon.wing@jhuapl.edu). Simon Wing acknowledges support from NSF grant AGS-1058456 and NASA grants (NNX13AE12G and NNX15AJ01G). Jay R. Johnson acknowledges support from NASA grants (NNH11AR071, NNX14AM27G, and NNX14AY20I), NSF grants (ATM0902730 and AGS-1203299), and DOE contract DE-AC02-09CH11466.

The Editor thanks Frederick Rich and an anonymous reviewer for their assistance in evaluating this paper.

References

- Baker, K. B., and S. Wing (1989), A new magnetic coordinate system for conjugate studies at high latitudes, *J. Geophys. Res.*, *94*(A7), 9139–9143, doi:10.1029/JA094iA07p09139.
- Block, L. P., and C.-G. Fälthammar (1991), Characteristics of magnetic-field aligned electric fields in the auroral acceleration region, in *Auroral Physics*, edited by C.-I. Meng, M. J. Rycroft, and L. A. Frank, pp. 109–118, Cambridge Univ. Press, New York.
- Burke, W. J., M. S. Gussenhoven, M. C. Kelley, D. A. Hardy, and F. J. Rich (1982), Electric and magnetic field characteristics of discrete arcs in the polar cap, *J. Geophys. Res.*, *87*(A4), 2431–2443, doi:10.1029/JA087iA04p02431.
- Chaston, C. C., J. W. Bonnell, L. M. Peticolas, C. W. Carlson, J. P. McFadden, and R. E. Ergun (2002), Driven Alfvén waves and electron acceleration, *Geophys. Res. Lett.*, *29*(11), 1535, doi:10.1029/2001GL013842.
- Damiano, P. A., and J. R. Johnson (2012), Electron acceleration in a geomagnetic Field Line Resonance, *Geophys. Res. Lett.*, *39*, L02102, doi:10.1029/2011GL050264.
- Echim, M. M., M. Roth, and J. De Keyser (2008), Ionospheric feedback effects on the quasi-static coupling between LBL and postnoon/evening discrete auroral arcs, *Ann. Geophys.*, *26*, 913–928.
- Fairfield, D. H., and J. D. Scudder (1985), Polar rain: Solar coronal electrons in the Earth's magnetosphere, *J. Geophys. Res.*, *90*(A5), 4055–4068, doi:10.1029/JA090iA05p04055.
- Fairfield, D. H., S. Wing, P. T. Newell, J. M. Ruohoniemi, J. T. Gosling, and R. M. Skoug (2008), Polar rain gradients and field-aligned polar cap potentials, *J. Geophys. Res.*, *113*, A10203, doi:10.1029/2008JA013437.
- Hardy, D. A., L. K. Schmitt, M. S. Gussenhoven, F. J. Marshall, H. C. Yeh, T. L. Shumaker, A. Hube, and J. Pantazis (1984), Precipitating Electron and Ion Detectors (SSJ/4) for the Block 5D/Flights 6-10 DMSP Satellites: Calibration and Data Presentation, *Rep. AFGL-TR-84-0317*, Air Force Geophys. Lab., Hanscom Air Force Base, Mass.
- Hoffman, R. A., R. A. Heelis, and J. S. Prasad (1985), A Sun-aligned arc observed by DMSP and AE-C, *J. Geophys. Res.*, *90*(A10), 9697–9710, doi:10.1029/JA090iA10p09697.
- Iijima, T., and T. A. Potemra (1976), The Amplitude distribution of field-aligned currents at northern high latitudes observed by Triad, *J. Geophys. Res.*, *81*(13), 2165–2174, doi:10.1029/JA081i013p02165.
- Johnson, J. R., and S. Wing (2015), The dependence of the strength and thickness of field-aligned currents on solar wind and ionospheric parameters, *J. Geophys. Res. Space Physics*, *120*, doi:10.1002/2014JA020312.
- Kitamura, N., K. Seki, Y. Nishimura, N. Terada, T. Ono, T. Hori, and R. J. Strangeway (2012), Photoelectron flows in the polar wind during geomagnetically quiet periods, *J. Geophys. Res.*, *117*, A07214, doi:10.1029/2011JA017459.
- Knight, L. (1973), Parallel electric fields, *Planet. Space Sci.*, *21*, 741–750.
- Lyons, L. (1980), Generation of large-scale regions of auroral currents, electric potentials, and precipitation by the divergence of the convection electric field, *J. Geophys. Res.*, *85*(A1), 17–24, doi:10.1029/JA085iA01p00017.
- Milan, S. E., B. Hubert, and A. Grocott (2005), Formation and motion of a transpolar arc in response to dayside and nightside reconnection, *J. Geophys. Res.*, *110*, A01212, doi:10.1029/2004JA010835.
- Newell, P. T., W. J. Burke, C.-I. Meng, E. R. Sanchez, and M. E. Greenspan (1991a), Identification and observations of the plasma mantle at low altitude, *J. Geophys. Res.*, *96*(A1), 34–45.
- Newell, P. T., S. Wing, C. I. Meng, and V. Sigillito (1991b), The auroral oval position, structure and intensity of precipitation from 1984 onwards: an automated on-line data base, *J. Geophys. Res.*, *96*(A4), 5877–5882, doi:10.1029/90JA02450.
- Newell, P. T., W. J. Burke, E. R. Sanchez, C.-I. Meng, M. E. Greenspan, and C. R. Clauer (1991c), The low-latitude boundary layer and the boundary plasma sheet at low altitude: Preon precipitation regions and convection reversal boundaries, *J. Geophys. Res.*, *96*(A12), 21,013–21,023, doi:10.1029/91JA01818.
- Rich, F. J., D. A. Hardy, and M. S. Gussenhoven (1985), Enhanced ionosphere-magnetosphere data from the DMSP satellites, *Eos Trans. AGU*, *66*, 513, doi:10.1029/EO066i026p00513.
- Spreiter, J. R., and S. S. Stahara (1985), Magnetohydrodynamic and gasdynamic theories for planetary bow waves, in *Collisionless Shocks in the Heliosphere: Reviews of Current Research*, *Geophys. Monogr. Ser.*, vol. 35B, edited by T. Tsurutani and R. G. Stone, pp. 85–107, AGU, Washington, D. C.

- Su, Y.-J., J. L. Horwitz, G. R. Wilson, P. G. Richards, D. G. Brown, and C. W. Ho (1998), Self-consistent simulation of the photoelectron-driven polar wind from 120 km to 9 R_E altitude, *J. Geophys. Res.*, *103*(A2), 2279–2296, doi:10.1029/97JA03085.
- Tsyganenko, N. A., and D. P. Stern (1996), Modeling the global magnetic field of the large-scale Birkeland current systems, *J. Geophys. Res.*, *101*(A12), 27,187–27,198, doi:10.1029/96JA02735.
- Watt, C. E. J., and R. Rankin (2009), Electron trapping in shear Alfvén waves that power the aurora, *Phys. Rev. Lett.*, *102*, 045002, doi:10.1103/PHYSREVLETT.102.045002.
- Wing, S., and P. T. Newell (1998), Central plasma sheet ion properties as inferred from ionospheric observations, *J. Geophys. Res.*, *103*(A4), 6785–6800, doi:10.1029/97JA02994.
- Wing, S., P. T. Newell, and T. G. Onsager (1996), Modeling the entry of magnetosheath electrons into the dayside ionosphere, *J. Geophys. Res.*, *101*(A6), 13,155–13,167, doi:10.1029/96JA00395.
- Wing, S., P. T. Newell, and J. M. Rouhoniemi (2001), Double cusp: Model prediction and observational verification, *J. Geophys. Res.*, *106*(A11), 25,571–25,593, doi:10.1029/2000JA000402.
- Wing, S., P. T. Newell, and C.-I. Meng (2005), Cusp modeling and observations at low altitude, *Surv. Geophys.*, *26*, 341–367, doi:10.1007/s10712-005-1886-0.
- Wing, S., S. Ohtani, P. T. Newell, T. Higuchi, G. Ueno, and J. M. Weygand (2010), Dayside field-aligned current source regions, *J. Geophys. Res.*, *115*, A12215, doi:10.1029/2010JA015837.
- Wing, S., S. Ohtani, J. R. Johnson, M. Echim, P. T. Newell, T. Higuchi, G. Ueno, and G. R. Wilson (2011), Solar wind driving of dayside field-aligned currents, *J. Geophys. Res.*, *116*, A08208, doi:10.1029/2011JA016579.
- Wing, S., M. Gkioulidou, J. R. Johnson, P. T. Newell, and C.-P. Wang (2013), Auroral particle precipitation characterized by the substorm cycle, *J. Geophys. Res. Space Physics*, *118*, 1022–1039, doi:10.1002/jgra.50160.
- Zhu, L., R. W. Schunk, and J. J. Sojka (1997), Polar cap arcs: A review, *J. Atmos. Sol. Terr. Phys.*, *59*, 1087–1126, doi:10.1016/S1364-6826(96)00113-7.